2 LAIDIG, W. D., HOLONYAK, N., JUN., CAMRAS, M. D., HESS, K., COLEMAN, J. J., DAPKUS, P. D., and BARDEEN, J.: 'Disorder of an AlAs–GaAs superlattice by impurity diffusion', *Appl. Phys. Lett.*, 1981, **38**, pp. 776–778
3 MARSH, J. H., HANSEN, S. I., BRYCE, A. C., and DE LA RUE, R. M.: 'Applications of neutral impurity disordering in fabricating low-loss optical waveguides and integrated waveguide devices', *Opt. Quantum Electron.*, 1991, **23**, pp. S941–S957
4 KAWABE, M., MATSUURA, N., SHIMIZU, N., HASEGAWA, F., and NANNICHI, Y.: 'Disordering of a Si-doped AlAs/GaAs superlattice by annealing', *Jpn. J. Appl. Phys.*, 1984, **23**, p. L623
5 THORNTON, R. L., MOSBY, W. J., and PAOLI, T. L.: 'Monolithic waveguide coupled cavity lasers and modulators fabricated by impurity induced disordering', *J. Lightwave Technol.*, 1988, **LT-6**, pp. 786–792
6 BAIRD, R. J., POTTER, T. J., LAI, R., KOTHIYAL, G. P., and BHATTACHARYA, P. K.: 'Impurity-induced layer disordering of $In_{0.53}Ga_{0.47}As/In_{0.52}Al_{0.48}As$ heterostructures', *Appl. Phys. Lett.*, 1988, **53**, pp. 2302–2304
7 RYS, A., SHIEH, Y., COMPAAN, A., YAO, H., and BHAT, A.: 'Pulsed laser annealing of GaAs implanted with Se and Si', *Opt. Eng.*, 1990, **29**, pp. 329–338
8 RALSTON, J., MORETTI, A. L., JAIN, R. K., and CHAMBERS, F. A.: 'Intermixing of $Al_xGa_{1-x}As/GaAs$ superlattices by pulsed laser irradiation', *Appl. Phys. Lett.*, 1987, **50**, pp. 1817–1819
9 EPLER, J. E., BURNHAM, R. D., THORNTON, R. L., PAOLI, T. L., and BASHAW, M. C.: 'Laser induced disordering of GaAs–AlGaAs superlattice and incorporation of Si impurity', *Appl. Phys. Lett.*, 1986, **49**, pp. 1447–1449
10 EPLER, J. E., BURNHAM, R. D., THORNTON, R. L., and PAOLI, T. L.: 'Low-threshold disorder-defined buried-heterostructure AlGaAs diode lasers by anisotropic diffusion of laser-incorporated Si', *Appl. Phys. Lett.*, 1987, **51**, pp. 731–733
11 MARSH, J. H., BRADSHAW, S. A., BRYCE, A. C., GWILLIAM, R., and GLEW, R. W.: 'Impurity induced disordering of GaInAs quantum wells with barriers of AlGaInAs or of GaInAsP', *IEEE J. Electron. Mater.*, 1991, **20**, pp. 973–978
12 PAPE, I. J., LI KAM WA, P., DAVID, J. P. R., CLAXTON, P. A., and ROBSON, P. N.: 'Disordering of $Ga_{0.47}In_{0.53}As/InP$ multiple quantum well layers by sulphur diffusion', *Electron. Lett.*, 1988, **24**, (19), pp. 1217–1218

RCS OF ELECTRICALLY LARGE TARGETS MODELLED WITH NURBS SURFACES

J. Pérez and M. F. Cátedra

Indexing terms: Radar cross-sections, Modelling

A technique is presented for the RCS computation of electrically large conducting bodies, modelled by NURBS patches, using physical optics (PO) and asymptotic expansion of integrals methods. The NURBS surfaces are transformed in Bezier patches to apply PO. Excellent accuracy is obtained.

Introduction: The radar cross-section (RCS) predictions of complex targets need a realistic modelling of the objects. At present the most popular target geometry modelling uses flat facets [1]. The geometric description is simple but has some disadvantages: it needs a very large number of facets in targets with complex geometries, artificial wedge appearance, etc.

An alternative is the NURBS (nonuniform rational B-spline) [2] surface design. It presents great advantages in the geometrical representation of complex targets. NURBS surfaces are parametric surfaces of arbitrary degree that provide

(i) good accuracy with a low number of patches

(ii) the capacity for every geometry to be modelled using a relatively low amount of information.

For these reasons NURBS modelling is currently used in many industries to represent complex bodies: aircraft, cars, etc.

PO techniques are used for RCS computation. Asymptotic analysis methods [3] are used to calculate the PO integral [4]. These techniques have a direct and very simple application in NURBS geometries.

Theory: Given an incident plane wave, under the far field approximation, the backscattering field of a general conducting surface S predicted by PO theory is given by

$$\vec{E}_s(\vec{r}) = -j\vec{E}_0 \frac{e^{+jkr}}{2\pi r} (\vec{K} \cdot \vec{I}) \tag{1}$$

$$\vec{I} = \int_s \hat{n}_s(\vec{r}') \cdot e^{2j\vec{K}\cdot\vec{r}'} \, ds' \tag{2}$$

where λ is the wavelength, $\vec{E}_0$ is the amplitude of the incident electric field, $\vec{K}$ is the wave vector, $\hat{n}_s$ is the normal vector at surface points, and $\vec{r}$ and $\vec{r}'$ are the observation and source points, respectively.

In this case the integral is extended over NURBS patches. NURBS surfaces are piecewise polynomial parametric surfaces normalised with a weight function. They are defined by two degrees (one for each parametric co-ordinate), a mesh of control points, a set of weights that define the weight function, and two knot vectors (one for each parametric co-ordinate).

The first step in solving the PO integral is to transform the NURBS surface into the corresponding rational Bezier patches [2] using the Cox–De Boor algorithm [5]. The mathematical treatment of Bezier surfaces is simple and numerically stable, and the surface point function computation and its derivatives is easy. The union of Bezier patches form the corresponding NURBS surface. They are polynomial parametric surfaces normalised with a weight function. A Bezier patch is defined by two degrees (one for each parametric co-ordinate), a mesh of control points and a set of associated weights. The continuity between Bezier patches is determined by the knot vectors of the corresponding NURBS surface.

The PO integral is computed as the sum of the integrals of the Bezier patches. A particular kind of Bezier surface is the plane facet. Its scattering field contribution is obtained using the Gordon method [6]. For curved surfaces, asymptotic expansion techniques are used for the PO integral computation. The PO integral under a general rational Bezier surface is given by

$$\vec{I} = \int_{u=0}^{u=1} \int_{v=0}^{v=1} \vec{r}_u(u, v) \times \vec{r}_v(u, v) e^{2j\vec{K}\cdot\vec{r}(u,v)} \, du \, dv \tag{3}$$

where the surface points are given by

$$\vec{r}(u, v) = \frac{\sum_{i=0}^{m} \sum_{j=0}^{n} w_{ij} \vec{b}_{ij} B_i^m(u) B_j^n(v)}{\sum_{i=0}^{m} \sum_{j=0}^{n} w_{ij} B_i^m(u) B_j^n(v)} \tag{4}$$

where m and n are the surface degrees, $\vec{b}_{ij}$ are the surface control points, w_{ij} are the control point weights, $B_i^m(u)$ and $B_j^n(v)$ are the Bernstein polynomials, and $\vec{r}_u(u, v)$ and $\vec{r}_v(u, v)$ are the derivative functions of eqn. 4.

To solve $\vec{I}$, the stationary phase method [3] is used. Thus

$$\vec{I} \simeq \pi e^{2j\vec{K}\cdot\vec{r}} (\vec{r}_u \times \vec{r}_v)[(\vec{K} \cdot \vec{r}_{uv})^2 - (\vec{K} \cdot \vec{r}_{uu})(\vec{K} \cdot \vec{r}_{vv})]^{-1/2} \tag{5}$$

where the function surface points $\vec{r}$ and its derivatives are evaluated at the stationary phase point; these are the specular points and are given by

$$\vec{K} \cdot \vec{r}_u(u_0, v_0) = 0$$
$$\vec{K} \cdot \vec{r}_v(u_0, v_0) = 0 \tag{6}$$

If over a Bezier surface more than one stationary phase point appears, the integral is the sum of the contributions due to all these points.

In the asymptotic integral computation, the contribution due to the finite domain is neglected. This is at least one order of magnitude smaller than the specular point contributions. Moreover, if the connection between patches is continuous in the parametric derivatives, the finite domain contributions are

cancelled. Under these assumptions the results obtained agree with geometrical optics (GO) [4] predictions.

When one of the second derivatives of the surface points equation is equal to zero, eqn. 5 is not valid. In this case it is possible to analytically solve the integral of one parametric co-ordinate; one of the principal curvatures is equal to zero for all the points. Two examples are cylinder and cone surfaces.

For example, if $\vec{r}_{vv}(u, v)$ is equal to zero, the stationary phase approximation is used to solve the integral over the 'u' co-ordinate:

$$\vec{I} = \int_{v=0}^{v=1} \vec{r}_u(u_0, v) \times \vec{r}_v(u_0, v) \sqrt{(\pi)} \times [-j\vec{K} \cdot \vec{r}_{uu}(u_0, v)]^{-1/2} e^{2j\vec{K} \cdot \vec{r}(u_0, v)}\, dv \quad (7)$$

In this case a stationary phase isoparametric segment appears with $u = u_0$ where u_0 is given by

$$\vec{K} \cdot \vec{r}_u(u_0, v) = 0 \quad (8)$$

The integral (eqn. 7) is solved analytically developing the amplitude term of the integral in the Taylor series about any value of $v = v_0$ (normally the domain mid-value):

$$\vec{I} = e^{jf_0} \sum_{n=0}^{N} \sum_{k=n}^{N} \frac{1}{(k-n)!\, n!} \vec{G}^{(k)} (-v_0)^{k-n} A_n \quad (9)$$

$$A_n = \int_0^1 v^n e^{jf_v v}\, dv = \frac{1}{jf_v} \left[\sum_{i=0}^{n} \frac{e^{jf_v}}{(-jf_v)^i (n-i)!} - \frac{1}{(-jf_v)^n} \right] \quad (10)$$

$$f_0 = 2\vec{K} \cdot \vec{r}(u_0, v_0) \qquad f_v = 2\vec{K} \cdot \vec{r}_v(u_0, v_0) \quad (11)$$

where $\vec{G}^{(k)}$ is the kth term of the amplitude Taylor series and N is the number of terms considered in the Taylor series.

Analogous expression are obtained when the patch verifies $\vec{r}_{uu}(u, v)$.

If over a Bezier surface more than one stationary phase segment appears, the global contribution is the sum of the contributions of the segments.

Results: The backscatter RCS values of an elliptic cylinder (Fig. 1), prolate spheroid (Fig. 2) and oblate spheroid (Fig. 3) are presented. All RCS values are normalised to 1 m^2. All the curves agree with GO predictions. RCS results are independent of the incident field polarisation.

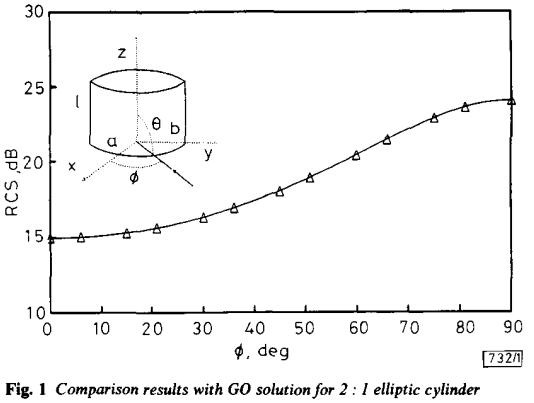

Fig. 1 *Comparison results with GO solution for 2 : 1 elliptic cylinder*
This is modelled using four NURBS patches
Incident direction is perpendicular to cylinder axis
——— GO
△ this method
$\theta = 90°$, $\lambda = 0{\cdot}1$ m, $l = 1$ m, $b = 1$ m, $a = 2$ m

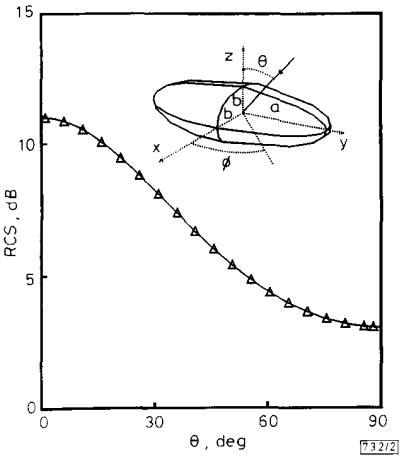

Fig. 2 *Comparison results with GO solution for 2 : 1 prolate spheroid modelled using light NURBS patches*
——— GO
△ this method
$a = 2$ m, $b = 1$ m, $\phi = 45°$

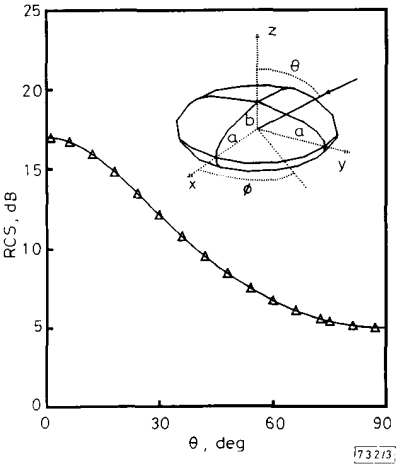

Fig. 3 *Comparison results with GO solution for 2 : 1 oblate spheroid modelled using eight NURBS patches*
——— GO
△ this method
$a = 2$ m, $b = 1$ m

Conclusions and future work: This work provides a general RCS computation method for electrically large targets modelled with NURBS surfaces. The method is efficient and accurate for targets without hard discontinuities between patches.

In the future, surface discontinuity contributions, curved wedge diffractions, creeping waves and second order effects (multiple reflections, patches hiding, etc.) will be considered.

Acknowledgment: This work was sponsored by DGT and CASA (No. Expte 115.88.12.781.00, TIC: 88-288E).

14th April 1992

J. Pérez and M. F. Cátedra (*Dpto. Electrónica, Universidad de Cantabria, Avda. Los Castros s/n. 39005 Santander, Spain*)

References

1 YOUSSEF, N. N.: 'Radar cross section of complex targets', *Proc. IEEE*, May 1989, 77, (5), pp. 722–734

2 FARIN, G.: 'Curves and surfaces for computer aided geometric design' (Academic Press, 1988)
3 SIROVICH, L.: 'Techniques of asymptotic analysis' (Springer-Verlag, New York, 1971)
4 RUCK, G. T., *et al.*: 'Radar cross section handbook' (Plenum Press, 1981)
5 BOHM, W.: 'Generating the Bezier points of B-spline curves and surfaces', *Computer Aided Design*, 1981, **13**, (16), pp. 365–366
6 GORDON, W. B.: 'Far field approximation of the Kirchhoff-Helmholtz representation of scattered fields', *IEEE Trans.*, July 1975, **AP-23**, pp. 864–876

EFFECT OF AMPLIFIER SATURATION ON ONE-SIDED BEAT SPECTRUM OF DRIVEN UNLOCKED OSCILLATOR

C. K. Campbell, P. J. Edmonson and P. M. Smith

Indexing terms: Oscillators, Amplifiers

Amplifier saturation converts the nominal one-sided beat spectrum of a driven unlocked oscillator into a two-sided one of asymmetric amplitude. It is shown that this can be attributed to the conversion of the circularly polarised phase-modulation vector to one with an elliptical component.

Introduction: The beat spectrum phenomenon of driven unlocked feedback oscillators with the form of Fig. 1 has been a subject of study for almost 50 years [1]. A study of such

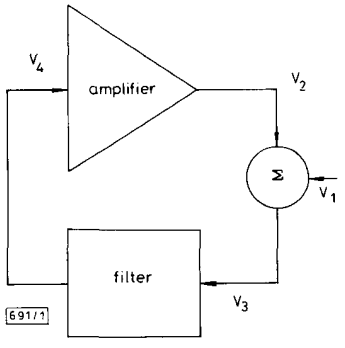

Fig. 1 *Basic feedback oscillator with injection drive*

behaviour in the unlocked state is important to an understanding of operation and bandwidth limitations of single-mode injection-locked electronic and laser oscillators [2], as well as multimode ones [3]. In theoretical studies reported to date [4, 5], the beat spectrum is derived as being ideally one-sided, with the carrier frequency lying between the beats and the injection frequency. Beat separations are dependent on the frequency difference between free-running and injection signals, and their relative amplitudes at the point of injection. These have previously been derived in terms of a circularly-polarised phase-modulation vector [1–5]. Experimentally, however, a two-sided beat spectrum of asymmetric amplitude and equal beat frequency separations is obtained with the degree of amplitude asymmetry decreasing with increasing injection amplitude. It is shown here that this can be explained by the conversion of the circularly-polarised phase-modulation vector to a partially elliptical one, as a result of inherent amplifier saturation which increases with injection power level.

Theory: Fig. 2*a* shows the vector relationships for the voltage components in the driven unlocked oscillator of Fig. 1. If signal distortion by the saturated amplifier is taken as insignificant (as in previous analyses), the phase modulation com-

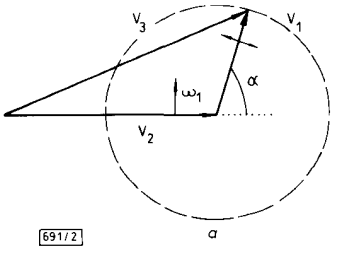

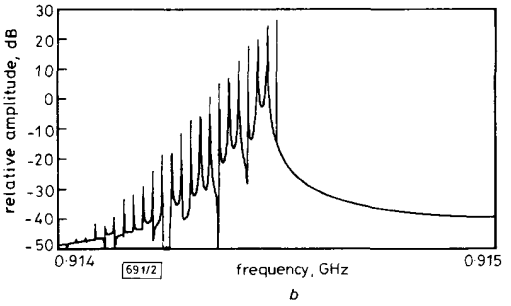

Fig. 2 *Circularly-polarised phase modulation vector with negligible amplifier saturation and one-sided beat spectrum for driven unlocked state, with $f_1 > f_0$ here (theoretical)*

a Phase modulation vector
b Beat spectrum

ponent V_1 is circularly-polarised, with time-dependent phase angle $\alpha(t)$ given by [1]

$$\alpha(t) = 2\tan^{-1}\left[\frac{1}{K} + \frac{\sqrt{(K^2-1)}}{K}\tan\frac{B(t-t_0)}{2}\sqrt{(K^2-1)}\right] \quad (1)$$

$$K = \frac{\Delta\omega_0}{B} = 2Q\frac{V_3}{V_1}\frac{\Delta\omega_0}{\omega_0} \quad (2)$$

where $\Delta\omega_0 = (\omega_0 - \omega_1) = 2\pi(f_0 - f_1)$, f_0 = 'free-running' frequency, f_1 = injection frequency, Q = resonator quality factor, t_0 = integration constant, $B = \omega_0 V_1/2QV_3$, and V_3 and V_1 are loop voltage vectors shown in Fig. 1. Under (assumed) negligible amplifier saturation, voltage vector V_1 is circularly polarised, with angular rotational frequency $\alpha(t)$. For $V_1 \ll V_3$ the resultant voltage response is $V_3 \simeq A \cdot \cos[\omega_1 t + \alpha(t)]$. Note that $\alpha(t)$ can have clockwise or anticlockwise rotation depending on the sign of $\Delta\omega_0$, thus placing the beat spectra above or below f_0. This gives the one-sided beat spectrum of Fig. 2*b*, with angular beat frequency separation $\Delta\omega_b = \Delta\omega_0 \cos(\theta)$, where $\sin(\theta) = K$, and $K < 1$ in the unlocked state [1, 4, 5].

Under significant amplifier saturation, however, V_1 will no longer have perfect circular polarisation, but will acquire an elliptical component as in Fig. 3*a*. Recalling that an elliptically-polarised vector may be decomposed into two oppositely-rotating circularly-polarised components of equal frequency but different amplitudes [6] (as in Fig. 3*b*), we obtain $V_3 \simeq C \cdot \cos[\omega_1 t + \alpha(t)] + D \cdot \cos[\omega_1 t - \alpha(t)]$ with $C/D > 1$, and the asymmetric beat spectrum of Fig. 3*c*.

Results: Fig. 4 exemplifies the experimental response for the driven unlocked oscillator, showing the typical asymmetric beat spectrum. This particular result was obtained for a surface acoustic wave (SAW) resonator oscillator with free-running frequency $f_0 = 914{\cdot}360$ MHz and injection at $f_1 = 914{\cdot}534$ MHz with $V_1/V_3 = -21$ dB. The frequency span in